npj | 2D Materials and Applications

www.nature.com/npj2dmaterials

ARTICLE OPEN

Overcoming the quantum efficiency-lifetime tradeoff of photocathodes by coating with atomically thin two-dimensional nanomaterials

Gaoxue Wang[1], Ping Yang[1], Nathan A. Moody[1] and Enrique R. Batista[1]

Photocathodes are key components of electron injectors for X-ray free electron laser and X-ray energy recovery linacs, which generate brilliant, ultrafast, and coherent X-rays for the exploration of matter with ultrahigh resolutions in both space and time. Whereas alkali-based semiconducting photocathodes display a higher quantum efficiency (QE) in the visible light spectrum than their metallic counterparts, their lifetimes are much shorter due to the high reactivity of alkali-based surfaces to the residual gases in the vacuum chamber. Overcoming the tradeoff between QE and lifetimes has been a great challenge in the accelerator community. Herein, based on ab initio density functional calculations, we propose an approach to overcome this tradeoff by coating with atomically thin two-dimensional (2D) nanomaterials. On one hand, the 2D coating layers can enhance the lifetimes of photocathodes by preventing the chemical reactions with the residual gases. On the other hand, the 2D coating layers can effectively engineer the work function of photocathodes, thus controlling their QE. A monolayer of insulating BN reduces the work function, whereas a monolayer of semi-metallic graphene or semiconducting molybdenum disulfide (MoS_2) increases the work function. This phenomenon originates from the induced interfacial dipoles. The reduction of work function by BN implies that it is capable of maintaining the high QE of semiconducting photocathodes in addition to enhance their lifetimes. This study advances our understandings on the surface chemistry of coated photocathodes and opens new technological avenues to fabricate photocathodes with high QE and longer lifetimes.

npj 2D Materials and Applications (2018)2:17 ; doi:10.1038/s41699-018-0062-6

INTRODUCTION

X-ray free electron laser (XFEL) and X-ray energy recovery linacs (XERL) are facilities for generating brilliant, ultrafast, and coherent X-rays with angstrom wavelength, which allows the experimental exploration of the structure and dynamics of atomic and molecular systems with ultrahigh resolutions in a broad range of research fields in physics, chemistry, biology, material science, and high energy density physics. Photocathodes are key components in the production of electron beams for XFEL and XERL.[1] Generally, there are two families of photocathodes: metal and semiconductor.[2] Metallic photocathodes such as copper, are very robust to chemical degradation but they have low quantum efficiency (QE) at the level of 10^{-4}–10^{-3}%. The low QE is due to the large work function, significant electron–electron scattering and strong surface reflection of incident light.[2] The poor QE of metallic photocathodes limits their usefulness in the production of high brightness electron beams. In contrast, alkali based semiconducting photocathodes, for examples, cesium antimony (Cs_3Sb), bialkali antimony (K_2CsSb), and negative electron affinity photocathodes such as gallium nitride (GaN-Cs), have lower work function and high QE, at the level of 1–20% in the visible light spectrum.[2,3] The limitation of these materials is that they are extremely reactive and even in the ultra-high vacuum (UHV) conditions inside the accelerators, their surfaces get quickly damaged, manifesting as decay in QE and short operational lifetimes.[3–7] Overcoming this tradeoff between QE and lifetimes has been a great challenge and a high priority in the accelerator community.

Various mechanisms lead to the short operational lifetimes of semiconducting photocathodes, for examples, ion back bombardment or thermally induced Cs loss and irreversible chemical reactions with oxygen containing residual gases.[3,5,8–11] All these processes result in the deviation from optimum Cs composition at the surface, which increases the work function and deteriorates the QE.[11] Therefore, suppressing or eliminating damage to the surfaces of semiconducting photocathodes is essential to extending their lifetimes. Passivating the highly reactive surfaces of semiconducting photocathodes with a coating layer, as illustrated in Fig. 1, is a conceptually attractive approach to prevent the damages to the surfaces. The coating layer can prohibit the irreversible chemical reactions with the residual gases and reduce the Cs loss due to the ion back bombardment. Efforts have been made in this direction to extend the lifetimes of photocathodes. For example, NaI, CsBr, and CsI films have been utilized to coat Cs_3Sb and K_2CsSb by Buzulutskov and Shefer.[12–15] It was found that these coating layers were able to protect photocathodes from oxidation provided that their thickness was greater than approximately 25 nm. Kimoto et al. have deposited 1–3 atomic layers of W or Cr to protect Cs_3Sb and they observed that the lifetime of Cs_3Sb was extended after W or Cr were oxidized to form W_2O_3 or Cr_2O_3 films.[16,17] Although the lifetime was elongated with these coating layers, the QE was dramatically

[1]Los Alamos National Laboratory, Los Alamos, NM 87545, USA
Correspondence: Enrique R. Batista (erb@lanl.gov)

Received: 25 January 2018 Revised: 2 May 2018 Accepted: 8 May 2018
Published online: 18 June 2018

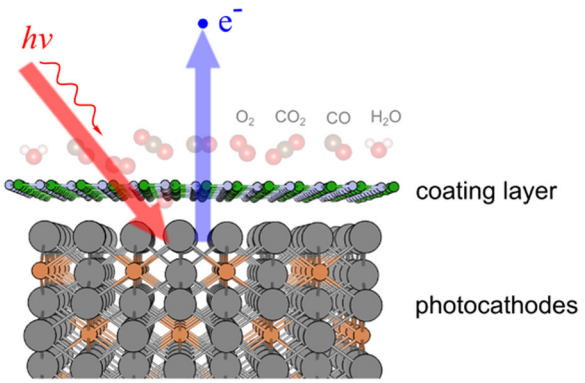

Fig. 1 Schematic illustration of passivating photocathodes with a coating layer to prevent the residual gas molecules from reaching the surface of photocathodes

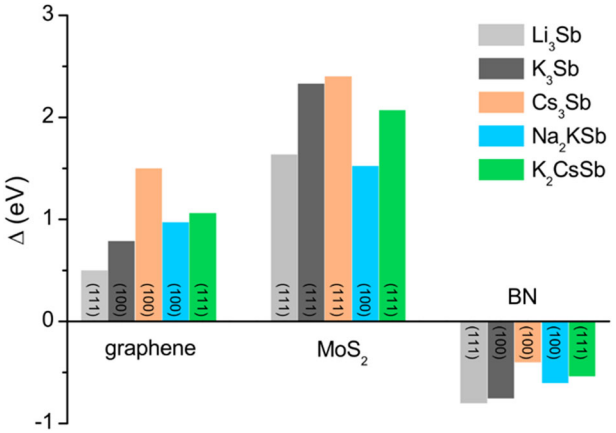

Fig. 2 Change of work function Δ upon monolayer of graphene, MoS_2 and BN is coated onto the (111) or (100) surface of semiconducting photocathodes

reduced due to the increase of the work function and the attenuation of excited photoelectrons in the thick coating films.

Ideally, an effective coating layer should be capable of protecting photocathodes without compromising the QE, thus the coating layer should meet the following criteria: (i) transparent to incident photons in the spectrum of the drive laser, (ii) inert and impermeable to the residual gases including O_2, H_2O, CO_2, CO, N_2, and H_2, (iii) thin enough to prevent the attenuation of excited photoelectrons in the coating films, (iv) low energy barrier for the electron to escape from the surface, namely the work function should not be increased to the point of stopping the photoelectrons from exiting the surfaces. Due to such rigorous criteria, an effective coating layer for semiconducting photocathodes has not been discovered yet. Single layers of two dimensional (2D) materials have atomic thickness, good transparency in the visible light spectrum, and impermeability to the gas molecules.[18–20] They satisfy most of the aforementioned criteria of an effective protective layer, therefore, are promising candidates for such applications. Very recently, graphene has been used to protect K_2CsSb and Cu.[21,22] It was reported that graphene was an excellent coating layer that increased the stability and QE of metallic Cu photocathode, while graphene was less effective for semiconducting K_2CsSb photocathode because of the increase of the work function, resulting in a significant reduction of QE.[21]

Despite these initial efforts on graphene coated photocathodes, no experimental and theoretical work has been undertaken to explore the possibility of using other 2D materials as coating layers. Herein, we present a theoretical study on 2D materials coated semiconducting photocathodes employing ab initio density functional calculations. The alkali antimonide photocathodes, including monoalkali antimonides Li_3Sb, K_3Sb, Cs_3Sb and bialkali antimonides Na_2KSb, K_2CsSb which have a high QE in the visible light spectrum but very short lifetimes of a few hours, are considered. Since the number of 2D materials is growing rapidly in recent years, it is a daunting task to computationally explore all these materials. However, with the aim of capturing the underlying physics and chemistry, we select graphene, molybdenum disulfide (MoS_2), and BN as coating layers due to the intrinsic difference in their electronic properties that are representative of most classes of the 2D materials: graphene is semi-metallic with zero band gap,[18,19] MoS_2 is semiconducting with a band gap of 1.8 eV,[23,24] and BN is insulating with a large band gap of 6.0 eV.[25]

We will demonstrate that the difference in the electronic properties of the coating layers leads to very different effects on the QE of the photocathodes. For the semi-metallic graphene and the semiconducting MoS_2, charge transfer from photocathodes to the conduction bands of the coating materials induces inward pointing dipoles which increase the work function. On the other hand, for monolayer BN, because of its large band gap, an outward dipole is formed at the interface originating from exchange repulsion, which decreases the work function. The results indicate that monolayer BN holds great promises as a coating layer that could not only protect the surfaces of semiconducting photocathodes but also maintain the high QE.

RESULTS

Change of work function

The work function is the minimum energy required for electrons to escape from a surface into the vacuum. In terms of Spicer's Three-Step model,[26] the work function is the main property that determines the escape rate of electrons into the vacuum. Thus, it is one of the most important parameters that determine the QE of photocathodes. The relaxed structures of graphene, MoS_2 and BN coated photocathodes are given in Figure S1 in the Supplementary Materials. The work function was calculated as $W = E_{vac} - E_F$, where E_{vac} is the planar averaged electrostatic potential in the vacuum region, and E_F is the Fermi energy as shown in Figure S2 in the Supplementary Materials. The change of work function $(\Delta = W_{coated} - W_{uncoated})$ of the Li_3Sb, K_3Sb, Cs_3Sb, Na_2KSb, and K_2CsSb photocathodes upon coating with graphene, MoS_2 and BN monolayer is summarized in Fig. 2. Remarkably, coating with the 2D materials could modify the work function of photocathodes up to 2.5 eV, and these coating layers display significantly different effects on the work function of photocathodes. Graphene and MoS_2 monolayer increase the work function by 0.5–1.5 eV and 1.5–2.5 eV, respectively. On the contrary, BN reduces the work function of these materials by −0.4 to −1.0 eV. Due to this reduction in the work function upon coating with monolayer BN, the QE of coated photocathodes is expected to be enhanced. In the following sections, we focus on Cs_3Sb which is one of the most experimentally characterized semiconducting photocathodes to elucidate the change of the work function and its effects on the QE of photocathodes.

Coating with monolayer graphene

As the firstly discovered 2D material, monolayer graphene can be fabricated with various methods including exfoliation from bulk graphite[19] and bottom–up strategies such as chemical vapor deposition (CVD).[27–29] Yamaguchi et al. have successfully coated graphene onto semiconducting K_2CsSb photocathode recently.[21] Figure 3 shows the calculated results of monolayer graphene on (001) surface of Cs_3Sb. After structural relaxation, the equilibrium distance (*d*) between Cs_3Sb and graphene is found to be 3.2 Å, and the binding energy of the coating graphene layer is −24.3 meV/ Å^2 (Figure S3 in the

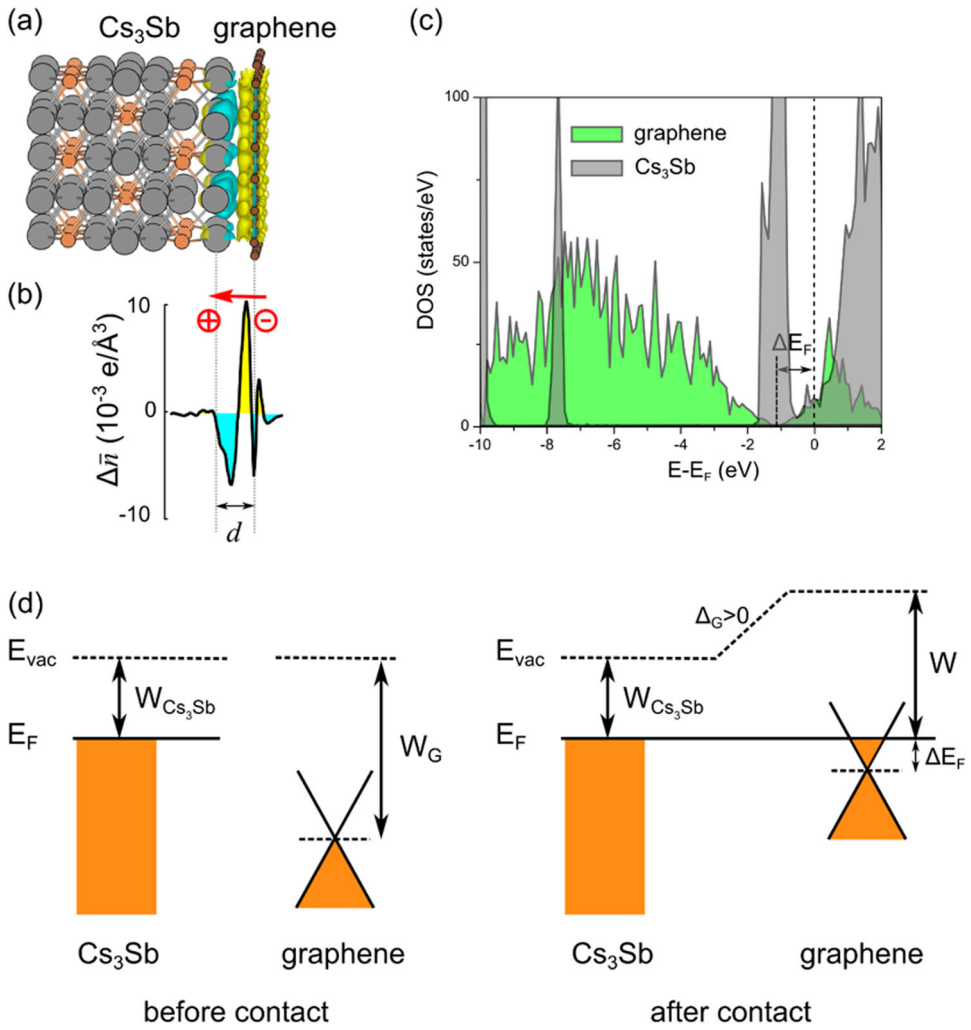

Fig. 3 Cs_3Sb (001) surface coated with monolayer graphene. **a** Charge density difference with isovalue of 0.001 e/bohr^3, the yellow region corresponds to charge accumulation, and blue region corresponds to charge depletion, **b** planar averaged charge density difference, the arrow inllustrates the induced dipole moment, **c** projected density of states of coated Cs_3Sb, and **d** band alignments before and after graphene in contact with the surface

Supplementary Materials). The binding energy is calculated as $E_b = \left(E_{Cs_3Sb\backslash graphene} - \left(E_{Cs_3Sb} + E_{graphene}\right)\right)/A$, where $E_{Cs_3Sb\backslash graphene}$ is the total energy of the combined system, E_{Cs_3Sb} and $E_{graphene}$ are the energy of separated surface and graphene, and A is the surface area.

To show the effects on the surface charge density upon coating with graphene, we calculate the charge density difference defined as $\Delta n(\boldsymbol{r}) = n_{Cs_3Sb\backslash graphene} - (n_{Cs_3Sb} + n_{graphene})$, where $n_{Cs_3Sb\backslash graphene}$ is the charge density of the combined system, n_{Cs_3Sb} and $n_{graphene}$ are the charge density of the separated Cs_3Sb surface and graphene, respectively. From the charge density difference in Fig. 3a, one can clearly see that charge is transferred from Cs_3Sb to graphene. The planar averaged charge density in Fig. 3b is obtained by taking the average of the charge density difference $\Delta n(\boldsymbol{r})$ in the lateral directions. We notice that the charge density increases above and below the plane of graphene indicating charge accumulation in the π^* bands of graphene. The projected density of states as shown in Fig. 3c and the band structure in Figure S4(a) in the Supplementary Materials also support the charge transfer from photocathodes to graphene. Graphene is therefore *n*-type doped as the Fermi level moves into the conduction bands of graphene. The charge transfer can be understood from the electronegativity of elements. Since Cs is one of the elements that have the lowest electronegativity on the periodic table, the transfer of Cs valence electrons to graphene is favorable. The charge transfer leads to the formation of a dipole moment at the interface of Cs_3Sb and graphene, and this dipole points into the surface, as illustrated by the arrow in Fig. 3b. The formation of the inward pointing dipole increases the work function to 3.5 eV, as obtained from the electrostatic potential profile (Figure S5(a) in the Supplementary Materials).

The band alignments before and after graphene comes in contact with the surface of Cs_3Sb are summarized in Fig. 3d. Before contact, free-standing graphene has zero band gap with linear energy dispersion at the Fermi level. Graphene has a larger work function ($W_G = 4.5$ eV) than the (001) surface of Cs_3Sb ($W_{Cs3Sb} = 2.01$ eV). Therefore, the Fermi level of Cs_3Sb is higher than some conduction bands of graphene. After coming in contact, charge transfers from the surface of Cs_3Sb to the empty conduction bands of graphene resulting in the shift of the Fermi level of graphene ($\Delta E_F = 1.0$ eV), and the work function of the Cs_3Sb surface is increased by $\Delta_G = 1.5$ eV. From these results, we conclude that whereas graphene can be a good protective layer for semiconducting photocathodes, it is expected to negatively affect the QE of Cs_3Sb due to the increase of the work function.

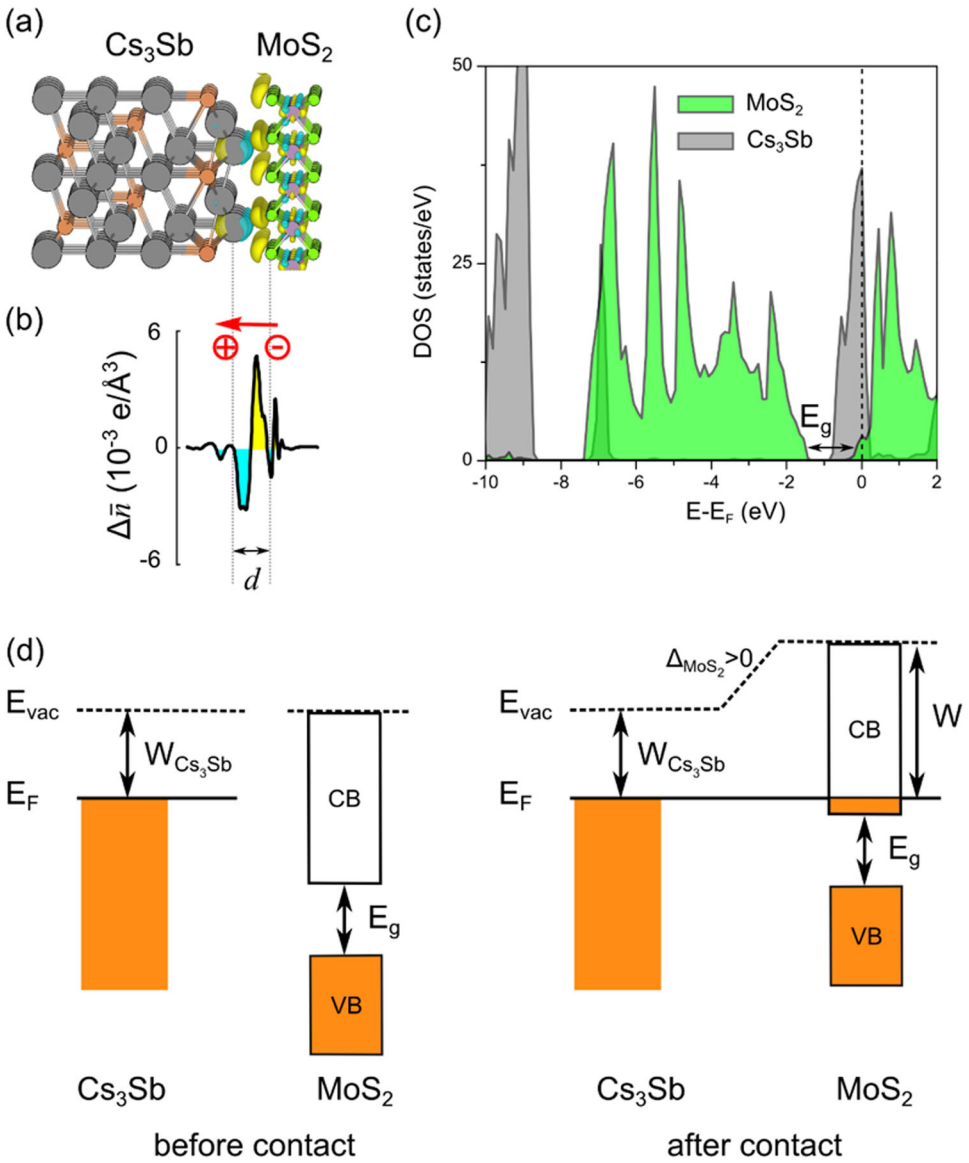

Fig. 4 Cs_3Sb (111) surface coated with monolayer MoS_2. **a** Charge density difference with isovalue of 0.0015 e/bohr^3, the yellow region corresponds to charge accumulation, and blue region corresponds to charge depletion, **b** planar averaged charge density difference, the arrow illustrates the induced dipole moment, **c** projected density of states of coated Cs_3Sb, and **d** band alignments before and after MoS_2 in contact with the surface. VB respresents valance bands, and CB conduction bands

Coating with monolayer MoS_2

Transition metal dichalcogenides (TMDCs) are a large family of layered materials with unique electronic and optical properties.[30] MoS_2 is a typical and most investigated member in the TMDCs family. Monolayer MoS_2 is a semiconductor with band gap of 1.8 eV.[24] The calculated results of MoS_2 on (111) surface of Cs_3Sb are shown in Fig. 4. The distance between the MoS_2 and the surface is 2.8 Å, and the binding energy is -25.4 meV/Å^2 comparable to that of graphene (Figure S3 in the Supplementary Materials). The charge density difference in Fig. 4a and its planar average in Fig. 4b show that charge is transferred from the surface of Cs_3Sb to MoS_2. As in the graphene coated photocathodes, a monolayer of MoS_2 leads to an induced dipole pointing into the surface. The Fermi level moves into the conduction bands of MoS_2 layer as seen from the projected density of states in Fig. 4c and the band stucture in Figure S4(b) in the Supplementary Materials. Such charge transfer can be explained by the band alignments of MoS_2 and Cs_3Sb in Fig. 4d. Before MoS_2 is in contact with the surface, the Fermi level of Cs_3Sb lies above the conduction band minimum of MoS_2. Since the conduction band minimum is lower than the Fermi level of Cs_3Sb, charge transfers from the Cs_3Sb surface to the conduction bands of MoS_2 at equilibrium upon contact. As a result, the work function of the coated surface increases to 4.4 eV as obtained from the electrostatic potential profile (Figure S5(b) in the Supplementary Materials). The large enhancement of the work function of $\Delta_{MoS2} = 2.4$ eV indicates that MoS_2 will dramatically reduce the QE of Cs_3Sb.

Coating with monolayer BN

Hexagonal BN monolayer, also known as 'white graphene', is isoelectronic to graphene,[31] however, their electronic properties are significantly different. Monolayer BN has a large band gap of approximately 6 eV, which allows it to be used as a dielectric in electronics. Also, it shows excellent stability in air and strong oxidation resistance.[20,32] This stability has been exploited using BN

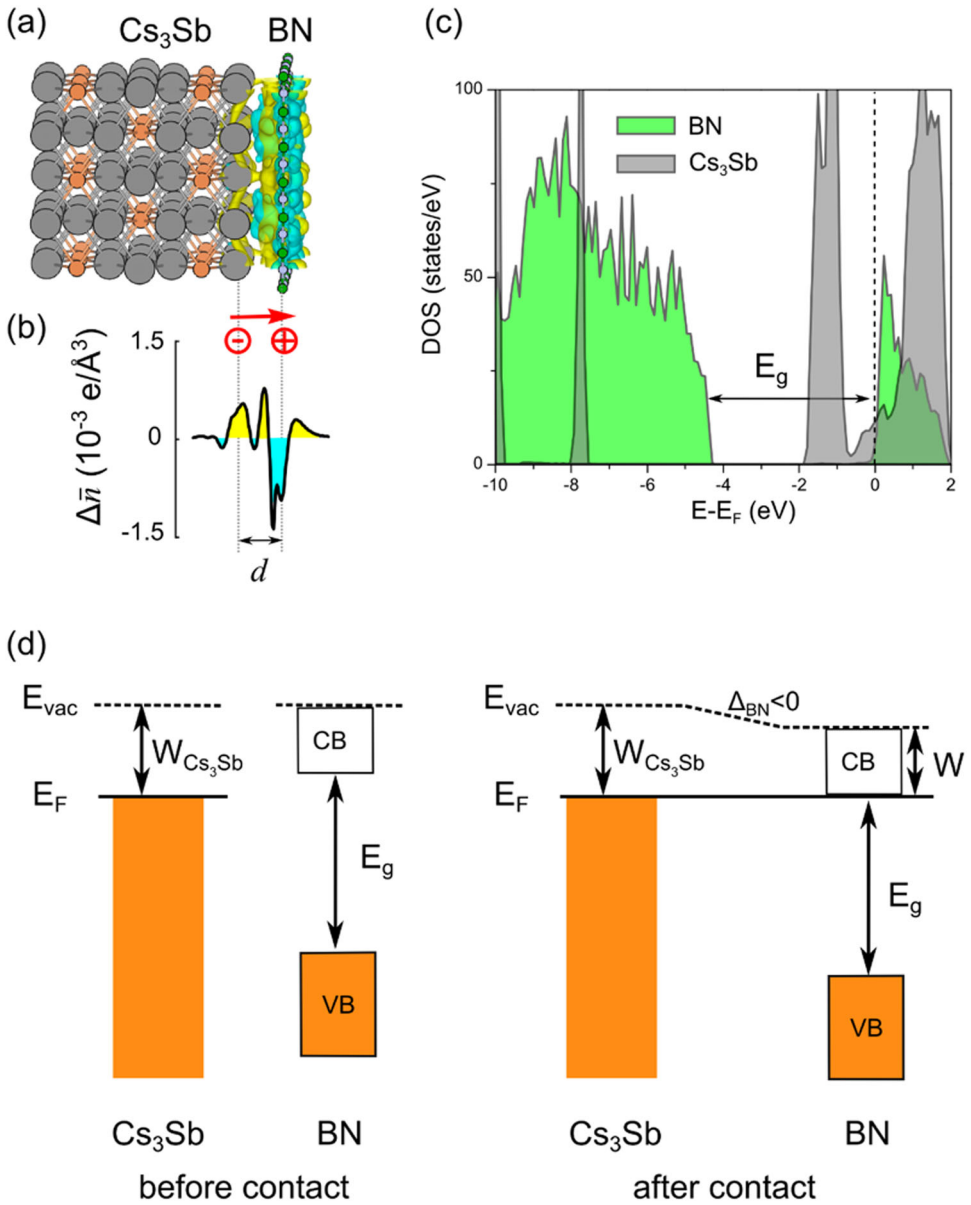

Fig. 5 Cs_3Sb (001) surface coated with monolayer BN. **a** Charge density difference with isovalue of 0.0002 e/bohr^3, the yellow region corresponds to charge accumulation, and blue region corresponds to charge depletion, **b** planar averaged charge density difference, the arrow illustrates the induced dipole moment, **c** projected density of states of coated Cs_3Sb, and **d** band alignments before and after BN in contact with the surface. VB respresents valance bands, and CB conduction bands

nanosheets as coating layers to protect polymers from oxidative corrosion.[33]

The calculated results of monolayer BN coated Cs_3Sb are shown in Fig. 5. The interaction of BN with Cs_3Sb surface shows obviously different characteristics from graphene and MoS_2 on the Cs_3Sb surface. Firstly, the binding of BN onto the surface of Cs_3Sb is much weaker than graphene and MoS_2. The equilibrium distance (*d*) between BN and Cs_3Sb is found to be 3.6 Å, and binding energy is −9.0 meV/Å^2 (Figure S3 in the Supplementary Materials). Secondly, we find that the induced dipole moment at the interface points to the opposite direction as compared to the graphene and MoS_2 coated surfaces. From the charge density difference in Fig. 5a and its planar average in Fig. 5b, one observes an accumulation of charge around the topmost Cs layer and a depletion around the side of BN layer resulting in an overall dipole moment that points out of the Cs_3Sb surface. Thirdly, upon charge rearrangement, the Fermi level moves closer to the conduction band minimum of BN (Fig. 5c and Figure S4(c) in the Supplementary Materials). This is in contrast to the case of graphene and MoS_2 where the Fermi level moves into its conduction bands. Lastly, the rearranged charge density is less than that in graphene and MoS_2 coated surfaces as can be seen from the maximum values in the planar averaged charge density difference in Fig. 5b, Fig. 3b and Fig. 4b, that is ~1.5×10^{-3} e/Å^3 for BN, ~10×10^{-3} e/Å^3 for graphene and ~5.0×10^{-3} e/Å^3 for MoS_2. All these facts imply different underlying mechanisms that control the interaction of BN with Cs_3Sb.

The differences lie in the electronic properties of the coating layers. Before BN is in contact with Cs_3Sb surface, free-standing BN has a large band gap (E_g) as illustrated in Fig. 5d. The Fermi level of Cs_3Sb lies below the conduction band minimum of BN. Since there are no BN conduction states below the Fermi level of Cs_3Sb, charge cannot transfer from Cs_3Sb to BN. Instead, the electron cloud of BN monolayer repels some charge between the surface of

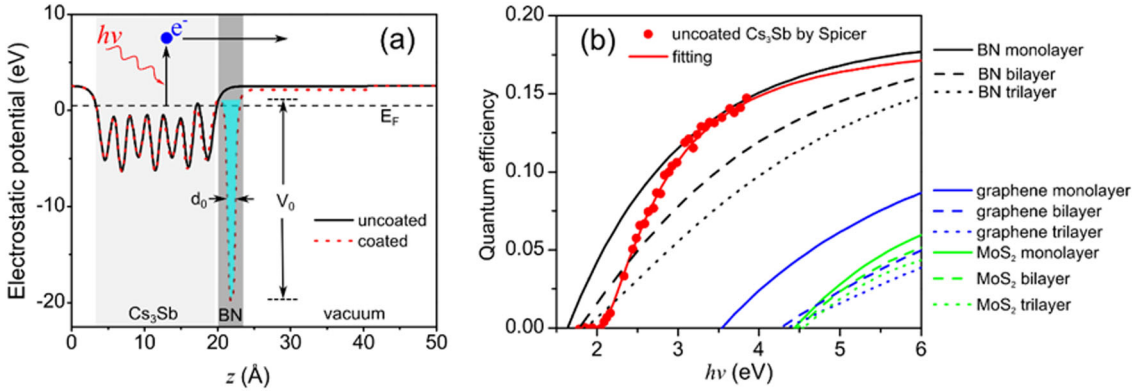

Fig. 6 **a** Electrostatic potential of uncoated and coated Cs_3Sb surface, the coating layer induces a potential well with width (d_0) and depth (V_0), **b** QE without and with the coating layers, the red dots are experimental results for uncoated Cs_3Sb reproduced from ref.[44]

Cs_3Sb and BN back into the slab when BN is in contact with Cs_3Sb. Accordingly, the electron density around the topmost Cs layer increases, and a dipole pointing outward the surface is formed. Such push-back effect originates from exchange repulsion (Pauli repulsion) and has been observed in organic molecules and BN adsorption on transition metals.[34–36] The outward pointing dipole decreases the energy barrier for electrons to escape into the vacuum, therefore, the work function of the coated surface is reduced to 1.6 eV as obtained from the electrostatic potential profile (Figure S5(c) in the Supplementary Materials). The reduction of the work function by $\Delta_{BN} = -0.4$ eV benefits the photoemission process. Thus, BN shows the potential to protect semiconducting photocathodes from degradation and increase the QE attributing to the reduction of the work function.

Effects on the QE

In order to estimate the QE of coated photocathodes we used the theoretical model proposed by Spicer.[26] According to this model,[26] the photoemission can be described by three successive steps: optical absorption, electron transport, and escape across the surface. The spectral QE of uncoated semiconducting photocathodes can be written as[37,38]

$$QE_{uncoated}(h\nu) = \frac{N_e}{N_{h\nu}} = \frac{1}{1+\frac{l_\alpha}{L(h\nu)}}\frac{h\nu - W}{h\nu} \quad (1)$$

where N_e is the number of emitted photoelectrons, $N_{h\nu}$ is the number of incident photons, l_α is the optical absorption length which is defined as the reciprocal of the absorption coefficient $l_\alpha = \frac{1}{\alpha(h\nu)}$, and $L(h\nu)$ is the scattering length of excited electrons.

The coating layer affects the QE of photocathodes in several ways. First of all, the optical absorbance in the coating layer reduces the number of photons that can reach the photocathodes. The optical absorption of monolayer graphene is around 2.3% in the visible light spectrum,[39,40] resulting in an optical transmission T_{opt} of 97.7%. MoS_2 monolayer possesses a higher absorption of 5–10% in the visible light region,[39] and the transmission T_{opt} is 90–95%. In contrast, because of its large band gap, a BN monolayer displays negligible absorbtance of visible light.[41,42] Secondly, the coating layer affects the transport of photoelectrons by creating a potential well at the surface as seen from the electrostatic potential profiles (Fig. 6a). The excited electrons will be scattered by this additional potential well before they escape into the vacuum. Inside the photocathodes, the electrostatic potential almost overlaps for the coated and uncoated surfaces (Fig. 6a), indicating the coating layer does not modify the electron transport in the bulk region. We estimated the transmission coefficient, T_e, approximating this part as a rectangular potential well[43]

$$\frac{1}{T_e} = 1 + \frac{1}{4}\frac{V_0^2}{E(E-V_0)}\sin^2\left(d_0\sqrt{\frac{2m\times 4\pi^2}{h^2}(E-V_0)}\right) \quad (2)$$

where V_0 and d_0 are the depth and width of the potential well as illustrated in Fig. 6a, m is the mass of excited electron, and E is the energy of the excited electron which is approximated with $E = E_F + h\nu$. The calculated depth V_0 is −20.3, −20.9, and −17.5 eV for BN, graphene and MoS_2 coated surfaces, respectively. The corresponding width (d_0) as mesured at the half maxium of the well is 1.09, 1.16, and 1.40 Å, respectively. The calculated transmission coefficient across the potential well induced by BN, graphene and MoS_2 is shown in Figure S6 in the Supplementary Materials. Lastly, the coating layer changes the work function which is directly reflected in the QE in Eq. 1.

Considering these effects of the coating layer, the spectral QE of coated semiconducting photocathodes can be expressed as

$$QE_{coated}(h\nu) = \frac{1}{1+\frac{l_\alpha}{L(h\nu)}}\frac{h\nu - W}{h\nu}T_{opt}^n T_e^n \quad (3)$$

where n is the number of coating layers. The term, $\frac{1}{1+\frac{l_\alpha}{L(h\nu)}}$, is related to the optical absorption and transport of excited electrons to the surface of Cs_3Sb. Since the coating layer is weakly absorbed on Cs_3Sb and it has little effects on the electrostatic potential inside the slab (Fig. 6a), it is a reasonable assumption that this term is unchanged by the coating layer. Therefore, we obtained $\frac{1}{1+\frac{l_\alpha}{L(h\nu)}}$ from the experimental data of the uncoated Cs_3Sb reported by Spicier,[26,44] and the results are shown in Figure S7 in the Supplementary Materials. It should be noted that this theoretical model has been employed to calculate the QE of graphene coated Cu photocathode yielding good agreements with the experimental data, the results will be reported elsewhere.

Since the optical transmission and electron transmission coefficient will decay with the number of coating layers, increasing the number of coating layers will decrease the QE. Therefore, an effective coating layer should be limited to a few layers. We have considered 1–3 layers of BN, graphene, and MoS_2 coating on Cs_3Sb. The corresponding work function is calculated and given in Table 1. The relaxed structures with 3 coating layers is shown in Figure S8 in the Supplementary Materials.

With all the parameters obtained above, we can obtain the QE of coated photocathodes using Eq. 3. The calculated QE is shown in Fig. 6b. For graphene and MoS_2 coated Cs_3Sb, the QE is significantly reduced and shifted to higher energy spectrum due to the increase of work function. Remarkably, BN coated Cs_3Sb maintains a high QE. Monolayer BN can even slightly enhance the QE of Cs_3Sb (solid black curve) in the visible light spectrum from

Table 1. Work function (in unit of eV) of coated Cs_3Sb with 1–3 layers of graphene, MoS_2, and BN

	Monolayer			Bilayer			Trilayer		
	E_F	E_{vac}	W	E_F	E_v	W	E_F	E_{vac}	W
Graphene	−1.12	2.38	3.50	0.08	4.34	4.26	0.54	4.88	4.34
MoS_2	−0.91	3.49	4.40	−0.10	4.38	4.48	0.90	5.44	4.54
BN	−0.19	1.41	1.60	0.98	2.76	1.78	1.50	3.35	1.85

~1.8 to ~3.1 eV. Although the QE of bilayer and trilayer BN coated Cs_3Sb (dashed black curve) is smaller than the uncoated one (red solid curve), they can still hold a high QE in the photon energy range of 2.0–6.0 eV. Considering the high QE of BN coated Cs_3Sb, a few layers of BN is a promissing coating material for semiconducting photocathodes.

DISCUSSION

Considering the rapid advances in synthesis techniques in recent years, atomically thin 2D materials with large areas can be fabricated nowadays. These 2D materials are promising and attractive as passivating layers for protecting alkali-based photocathodes against degradation due to reactions with residual gases, and providing a technological path toward extending their lifetimes. Based on ab initio density functional calculations, we demonstrate that besides protecting the surfaces a few layers of BN also reduces the work function of alkali-based photocathodes. This reduction of the work function is ascribed to the formation of the outward pointing dipole moments at the interfaces. Monolayer of BN surprisingly maintains the high QE making it an ideal coating material for alkali-based semiconducting photocathodes.

Although a few layers of graphene or MoS_2 can also be protective to semiconducting photocathodes, they are found to increase their work function. The increase of the work function is due to charge transfer from the photocathodes to the conduction bands of semi-metallic graphene and semiconducting MoS_2. Such charge transfer induces the formation of inward pointing dipoles which stop the electrons from escaping from the surfaces, thus significantly suppressing the QE. The theoretical explorations in this work not only advance the understandings on the physics and chemistry of coated photocathodes, but also open new avenues to overcome the QE-lifetime tradeoff of photocathodes, which is important for fabrication of high performance photocathodes for electron-beam applications.

METHODS

Electronic structure calculations

Our calculations were performed with the use of density functional theory (DFT) and projector augmented-wave (PAW) method[45] as implemented in the Vienna ab initio Simulation Package (VASP).[46] The generalized gradient approximation (GGA) of Perdew-Burke-Ernzerhof (PBE)[47] functional was used to represent the exchange–correlation interaction. Since PBE functional could not capture the van der Waals (vdW) interactions in graphene and BN layers,[48,49] the DFT-D3 method of Grimme[50] was included in the calculations. Plane wave basis sets with a cutoff energy of 500 eV were employed.[45] The energy convergence was set to 10^{-6} eV and the residual force on each atom was smaller than 0.01 eV/Å for structural relaxations.

The alkali antimonide photocathodes have a cubic structure with the space group of Fm-3m (No. 225 of the international tables for crystallography).[51] The calculated lattice constants for these photocathodes are listed in Table 1 in the Supplementary Materials, which are in agreement with the experimental reports. The calculated lattice constants for a monolayer of graphene (2.47 Å), MoS_2 (3.15 Å) and BN (2.51 Å) are in excellent agreement with the experimental values of 2.46,[52] 3.18 Å[23,53] and 2.51,[54] respectively.

Surfaces of photocathodes

The surfaces of photocathodes were represented with slab models in the 3-dimensional periodic-boundary-condition simulation with a vacuum gap in the direction normal to the surface. In the supercell, the vacuum distance normal to the slab was larger than 30 Å to eliminate the interactions between the replicas due to the periodic boundary conditions. The dipole correction was included to nullify the artificial field imposed on the slab by the periodic boundary conditions.[55] The surfaces were terminated with alkali atoms, which were the most stable surface configurations according to our previous work.[11]

Coated photocathodes

To coat the surfaces with 2D materials, large supercells were chosen to get commensurate structures between the photocathodes and coating layers. Note that the 2D materials were coated on different crystalline surfaces of photocathodes depending on the matching of their lattice constants. For example, for Cs_3Sb, a rectangular 2×2 supercell of the (001) surface with size of 12.95×12.95 Å^2 matched with the $5\times3\sqrt{3}$ supercell of monolayer graphene and BN with size of 12.35×12.83 Å^2 and 12.55×13.04 Å^2, respectively; a hexagonal 1×1 supercell of the (111) surface of Cs_3Sb with a size of 6.47×6.47 (60°) Å^2 matched with the 2×2 supercell of monolayer MoS_2 with a size of 6.30×6.30 (60°) Å^2. The supercells for other coated photocathodes were listed in Table S2 in the Supplementary Materials. The reciprocal space was sampled by Monkhorst-Pack k points in the Brillouin zone with a grid of $(3\times3\times1)$ for the (001) surface and $(7\times7\times1)$ for the (111) surface, respectively. During structural optimization, three atomic layers at the bottom of the slabs were fixed to the bulk value and the rest of the atoms were fully relaxed. The relaxed structures of the coated photocathodes are given in Figure S1 in the Supplementary Materials.

Work function

The work function was calculated as $W = E_{vac} - E_F$, where E_{vac} was the planar averaged electrostatic potential in the vacuum region, and E_F was the Fermi energy. It should be noted that although the studied bulk semiconducting photocathodes have band gaps, the surfaces of these materials have metallic states due to dangling bonds. The Fermi level of the metallic surfaces was used to calculate the work function. Examples of planar averaged electrostatic potential profiles can be found in Figures S2 (a) and S2(b) in the Supplementary Materials for the (001) and (111) surfaces of Cs_3Sb. The thicknesses of the slab that we used for the calculations were larger than 10 Å to converge the work function within 0.01 eV (see Figure S2(c) in the Supplementary Materials for Cs_3Sb). The calculated work function of uncoated alkali antimonide photocathodes is in the range of 2–3 eV depending on the surfaces as shown in Table S3 in the Supplementary Materials.

Previous studies have suggested that the local density approximation (LDA) empirically gives a reasonable bonding and work function of graphene and BN adsorption on metal surfaces,[56,57] although the vdW interactions are not properly described at LDA level of theory. Thus, we also compared our results with the LDA (Table S4 in the Supplementary Materials). Both PBE plus DFT-D3 and LDA were found to give similar results on the change of work function. Moreover, it is well-known that band gaps of semiconductors are underestimated at GGA-DFT level of theory, hence, we further calculated the band alignments with the more accurate Heyd-Scuseria-Ernzerh (HSE06) hybrid functional[58–60] as shown in Figure S9 in the Supplementary Materials. The band gaps of MoS_2 and BN monolayer were increased to 2.0 and 5.5 eV, respectively, with the HSE06 functional. The band gap of MoS_2 monolayer is overestimated as compared to the experimental value, which is in agreement with previous reports.[61,62] However, the relative positions of the Fermi level of photocathodes to the conduction band minimum of the coating layer is not changed with the HSE06 functional. Therefore, the physics described in this paper should not be affected by using a different functional. Unless stated otherwise, the results from PBE plus DFT-D3 were reported in the main context.

Data availability

The data that support the findings of this study are available upon reasonable request from G.W. (email: gaoxuew@lanl.gov), P.Y. (email: pyang@lanl.gov) and E.R.B. (email: erb@lanl.gov).

ACKNOWLEDGEMENTS

The authors gratefully acknowledge funding for this project from the Laboratory Directed Research and Development program of Los Alamos National Laboratory (LANL) under project 20150394DR. G.W. thanks the Director's Postdoc Fellow from LANL. Los Alamos National Laboratory is operated by Los Alamos National Security, LLC, for the National Nuclear Security Administration of U.S. Department of Energy (contract DE-AC52-06NA25396). We thank the access to computational resources for this project from the Environmental Molecular Sciences Laboratory of Pacific Northwest National Laboratory in the cascade cluster and LANL's institutional computer, wolf cluster.

AUTHOR CONTRIBUTIONS

N.A.M. and E.R.B. initiated the project. E.R.B. conceived the idea of coating photocathodes. G.W. did the calculations and analyzed the results along with P.Y. and E.R.B. G.W. wrote the manuscript. P.Y., N.A.M., and E.R.B. revised the manuscript.

ADDITIONAL INFORMATION

Supplementary information accompanies the paper on the *npj 2D Materials and Applications* website (https://doi.org/10.1038/s41699-018-0062-6).

Competing interests: N.A.M. owns a patent on the concept of graphene protection of chemically reactive films. The other authors declare no competing interests.

Publisher's note: Springer Nature remains neutral with regard to jurisdictional claims in published maps and institutional affiliations.

REFERENCES

1. Carlsten, B. E. et al. New source technologies and their impact on future light sources. *Nucl. Instrum. Methods Phys. Res. Sect. A Accel. Spectrometers Detect. Assoc. Equip.* **622**, 657–668 (2010).
2. Xiang, R. & Teichert, J. Photocathodes for high brightness photo injectors. *Phys. Procedia* **77**, 58–65 (2015).
3. Michelato, P. Photocathodes for RF photoinjectors. *Nucl. Instrum. Methods Phys. Res. Sect. A Accel. Spectrometers Detect. Assoc. Equip.* **393**, 455–459 (1997).
4. Pavlenko, V., Liu, F., Hoffbauer, M. A., Moody, N. A. & Batista, E. R. Kinetics of alkali-based photocathode degradation. *AIP Adv.* **6**, 115008 (2016).
5. Danielson, L. R., Lee, C. & Oettinger, P. E. Laser illuminated high current photocathodes. *Appl. Surf. Sci.* **16**, 257–267 (1983).
6. Pastuszka, S., Terekhov, A. S. & Wolf, A. 'Stable to unstable' transition in the (Cs, O) activation layer on GaAs (100) surfaces with negative electron affinity in extremely high vacuum. *Appl. Surf. Sci.* **99**, 361–365 (1996).
7. Chanlek, N. et al. The degradation of quantum efficiency in negative electron affinity GaAs photocathodes under gas exposure. *J. Phys. D. Appl. Phys.* **47**, 055110 (2014).
8. Springer, R. W. & Cameron, B. J. Photocathode transfer and storage techniques using alkali vapor feedback control. *Nucl. Instrum. Methods Phys. Res. Sect. A Accel. Spectrometers Detect. Assoc. Equip.* **318**, 396–400 (1992).
9. Decker, R. Decay of S-20 photocathode sensitivity due to ambient gases. *Adv. Electron Electron Phys.* **28**, 357 (1969).
10. Sommer, A. Stability of photocathodes. *Appl. Opt.* **12**, 90–92 (1973).
11. Wang, G., Pandey, R., Moody, N. A. & Batista, E. R. Degradation of alkali-based photocathodes from exposure to residual gases: a first-principles study. *J. Phys. Chem. C.* **121**, 8399–8408 (2017).
12. Buzulutskov, A., Breskin, A., Chechik, R., Prager, M. & Shefer, E. Protection of cesium-antimony photocathodes. *Nucl. Instrum. Methods Phys. Res. Sect. A Accel. Spectrometers Detect. Assoc. Equip.* **387**, 176–179 (1997).
13. Buzulutskov, A., Shefer, E., Breskin, A., Chechik, R. & Prager, M. The protection of KCsSb photocathodes with CsBr films. *Nucl. Instrum. Methods Phys. Res. Sect. A Accel. Spectrometers Detect. Assoc. Equip.* **400**, 173–176 (1997).
14. Shefer, E., Breskin, A., Buzulutskov, A., Chechik, R. & Prager, M. Composite photocathodes for visible photon imaging with gaseous photomultipliers. *Nucl. Instrum. Methods Phys. Res. Sect. A Accel. Spectrometers Detect. Assoc. Equip.* **419**, 612–616 (1998).
15. Shefer, E. et al. Coated photocathodes for visible photon imaging with gaseous photomultipliers. *Nucl. Instrum. Methods Phys. Res. Sect. A Accel. Spectrometers Detect. Assoc. Equip.* **433**, 502–506 (1999).
16. Kimoto, T., Arai, Y. & Ren, X. Lifetime test of photoemission from Cs_3Sb photocathode coated with W or Cr film. *Appl. Surf. Sci.* **284**, 657–670 (2013).
17. Kimoto, T., Arai, Y. & Nagayama, K. Experiments for improving fabrication, recovery and surface-protection of Cs_3Sb photocathode. *Appl. Surf. Sci.* **393**, 474–485 (2017).
18. Novoselov, K. S. et al. Electric field effect in atomically thin carbon films. *Science* **306**, 666–669 (2004).
19. Geim, A. K. & Novoselov, K. S. The rise of graphene. *Nat. Mater.* **6**, 183–191 (2007).
20. Wang, G., Pandey, R. & Karna, S. P. Physics and chemistry of oxidation of two-dimensional nanomaterials by molecular oxygen. *Wiley Interdiscip. Rev. Comput. Mol. Sci.* **7**, e1280 (2017).
21. Yamaguchi, H. et al. Active bialkali photocathodes on free-standing graphene substrates. *NPJ 2D Mater. Appl.* **1**, 12 (2017).
22. Liu, F. et al. Single layer graphene protective gas barrier for copper photocathodes. *Appl. Phys. Lett.* **110**, 041607 (2017).
23. Radisavljevic, B., Radenovic, A., Brivio, J., Giacometti, iV. & Kis, A. Single-layer MoS_2 transistors. *Nat. Nanotechnol.* **6**, 147–150 (2011).
24. Mak, K. F., Lee, C., Hone, J., Shan, J. & Heinz, T. F. Atomically thin MoS_2: a new direct-gap semiconductor. *Phys. Rev. Lett.* **105**, 136805 (2010).
25. Kim, K. K. et al. Synthesis of monolayer hexagonal boron nitride on Cu foil using chemical vapor deposition. *Nano. Lett.* **12**, 161–166 (2011).
26. Spicer, W. E. Photoemissive, photoconductive, and optical absorption studies of alkali-antimony compounds. *Phys. Rev.* **112**, 114–122 (1958).
27. Yu, Q. et al. Graphene segregated on Ni surfaces and transferred to insulators. *Appl. Phys. Lett.* **93**, 113103 (2008).
28. Reina, A. et al. Large area, few-layer graphene films on arbitrary substrates by chemical vapor deposition. *Nano. Lett.* **9**, 30–35 (2008).
29. Kang, K. et al. High-mobility three-atom-thick semiconducting films with wafer-scale homogeneity. *Nature* **520**, 656–660 (2015).
30. Wang, Q. H., Kalantar-Zadeh, K., Kis, A., Coleman, J. N. & Strano, M. S. Electronics and optoelectronics of two-dimensional transition metal dichalcogenides. *Nat. Nanotechnol.* **7**, 699–712 (2012).
31. Watanabe, K., Taniguchi, T. & Kanda, H. Direct-bandgap properties and evidence for ultraviolet lasing of hexagonal boron nitride single crystal. *Nat. Mater.* **3**, 404–409 (2004).
32. Li, L. H., Cervenka, J., Watanabe, K., Taniguchi, T. & Chen, Y. Strong oxidation resistance of atomically thin boron nitride nanosheets. *ACS Nano* **8**, 1457–1462 (2014).
33. Yi, M., Shen, Z., Zhao, X., Liang, S. & Liu, L. Boron nitride nanosheets as oxygen-atom corrosion protective coatings. *Appl. Phys. Lett.* **104**, 143101 (2014).
34. Morikawa, Y., Ishii, H. & Seki, K. Theoretical study of n-alkane adsorption on metal surfaces. *Phys. Rev. B* **69**, 041403 (2004).
35. Romaner, L., Nabok, D., Puschnig, P., Zojer, E. & Ambrosch-Draxl, C. Theoretical study of PTCDA adsorbed on the coinage metal surfaces, Ag (111), Au (111) and Cu (111). *New J. Phys.* **11**, 053010 (2009).
36. Bokdam, M., Brocks, G., Katsnelson, M. I. & Kelly, P. J. Schottky barriers at hexagonal boron nitride/metal interfaces: a first-principles study. *Phys. Rev. B* **90**, 085415 (2014).
37. Spicer, W. E. & Herrera-Gomez, A. Modern theory and applications of photocathodes. *Proc. SPIE* **2022**, 18 (1993).
38. Kirschner, H. *Spectral Quantum Efficency Measurements on Cs–K–Sb Photocathodes for the Energy-Recovery Linac Test Facility bERLinPro*. (2017).
39. Bernardi, M., Palummo, M. & Grossman, J. C. Extraordinary sunlight absorption and one nanometer thick photovoltaics using two-dimensional monolayer materials. *Nano. Lett.* **13**, 3664–3670 (2013).
40. Nair, R. R. et al. Fine structure constant defines visual transparency of graphene. *Science* **320**, 1308–1308 (2008).
41. Sharma, S., Kalita, G., Vishwakarma, R., Zulkifli, Z. & Tanemura, M. Opening of triangular hole in triangular-shaped chemical vapor deposited hexagonal boron nitride crystal. *Sci. Rep.* **5**, 10426 (2015).
42. Han, J., Lee, J.-Y., Kwon, H. & Yeo, J.-S. Synthesis of wafer-scale hexagonal boron nitride monolayers free of aminoborane nanoparticles by chemical vapor deposition. *Nanotechnology* **25**, 145604 (2014).
43. Liboff, R. L. *Introductory Quantum Mechanics* (San Francisco, CA: Addison-Wesley, 2003).
44. Jensen, K. L. et al. Theory of photoemission from cesium antimonide using an alpha-semiconductor model. *J. Appl. Phys.* **104**, 044907 (2008).
45. Kresse, G. & Joubert, D. From ultrasoft pseudopotentials to the projector augmented-wave method. *Phys. Rev. B* **59**, 1758 (1999).
46. Kresse, G. & Furthmüller, J. Efficiency of ab-initio total energy calculations for metals and semiconductors using a plane-wave basis set. *Comput. Mater. Sci.* **6**, 15–50 (1996).
47. Perdew, J. P., Burke, K. & Ernzerhof, M. Generalized gradient approximation made simple. *Phys. Rev. Lett.* **77**, 3865 (1996).
48. Sachs, B., Wehling, T., Katsnelson, M. & Lichtenstein, A. Adhesion and electronic structure of graphene on hexagonal boron nitride substrates. *Phys. Rev. B* **84**, 195414 (2011).

49. Giovannetti, G., Khomyakov, P. A., Brocks, G., Kelly, P. J. & Van Den Brink, J. Substrate-induced band gap in graphene on hexagonal boron nitride: Ab initio density functional calculations. *Phys. Rev. B* **76**, 073103 (2007).
50. Grimme, S. Semiempirical GGA-type density functional constructed with a long-range dispersion correction. *J. Comput. Chem.* **27**, 1787–1799 (2006).
51. Hahn, T. (ed.) *International Tables for Crystallography, Reidel Publishing Company*, Boston (1983).
52. Ohta, T., Bostwick, A., Seyller, T., Horn, K. & Rotenberg, E. Controlling the electronic structure of bilayer graphene. *Science* **313**, 951–954 (2006).
53. Kan, M. et al. Structures and phase transition of a MoS_2 monolayer. *J. Phys. Chem. C.* **118**, 1515–1522 (2014).
54. Meyer, J. C., Chuvilin, A., Algara-Siller, G., Biskupek, J. & Kaiser, U. Selective sputtering and atomic resolution imaging of atomically thin boron nitride membranes. *Nano. Lett.* **9**, 2683–2689 (2009).
55. Bengtsson, L. Dipole correction for surface supercell calculations. *Phys. Rev. B* **59**, 12301–12304 (1999).
56. Khomyakov, P. et al. First-principles study of the interaction and charge transfer between graphene and metals. *Phys. Rev. B* **79**, 195425 (2009).
57. Giovannetti, G. et al. Doping graphene with metal contacts. *Phys. Rev. Lett.* **101**, 026803 (2008).
58. Heyd, J., Scuseria, G. E. & Ernzerhof, M. Hybrid functionals based on a screened Coulomb potential. *J. Chem. Phys.* **118**, 8207–8215 (2003).
59. Heyd, J., Peralta, J. E., Scuseria, G. E. & Martin, R. L. Energy band gaps and lattice parameters evaluated with the Heyd-Scuseria-Ernzerhof screened hybrid functional. *J. Chem. Phys.* **123**, 174101 (2005).
60. Kudin, K. N., Scuseria, G. E. & Martin, R. L. Hybrid density-functional theory and the insulating gap of UO_2. *Phys. Rev. Lett.* **89**, 266402 (2002).
61. Li, Y. G., Li, Y. L., Araujo, C. M., Luo, W. & Ahuja, R. Single-layer MoS_2 as an efficient photocatalyst. *Catal. Sci. & Technol.* **3**, 2214–2220 (2013).
62. Li, Y. G., Li, Y. L., Sa, B. S. & Ahuja, R. Review of two-dimensional materials for photocatalytic water splitting from a theoretical perspective. *Catal. Sci. & Technol.* **7**, 545–559 (2017).